A Model for Mercury Orificed Hollow Cathodes: Theory and Experiment

Daniel E. Siegfried* and Paul J. Wilbur†
Colorado State University, Fort Collins, Colorado

The model outlined here provides a useful qualitative description of the basic physical processes taking place within a mercury orificed hollow cathode and can predict, to first order, important cathode operating parameters such as emission length and insert temperature. The analytical formulation of the model is based on the concept of an idealized "ion production region," which is defined as the volume circumscribed by the emitting portion of the insert. The energy exchange mean free path for primary electrons is used as a criterion for determining the length L_e of this region. An ion production region aspect ratio D/L_e of 2 is suggested as a design criterion for minimizing the keeper voltage. The model accounts for electrons produced in the ion production region by surface emission and volume ionization. Surface and volume energy balances are used to predict plasma density and plasma potential in this region. An empirical relation is presented that can be used to estimate cathode internal pressure (a necessary input to the model) from the discharge current and cathode orifice diameter. Calculations based on the model are compared with experimental results.

Nomenclature

a_0 = theoretical constant, 1.2×10^6 A/m$^2 \cdot$K^2
A_c = area of end boundary of ion production region, m^2
A_e = insert emission area, m^2
A_s = total surface area of ion production
d_0 = orifice diameter, mm
D = insert inner diameter, m
e = electronic charge, C
E = electric field at insert surface, V/m
I_D = total discharge current, A
I_e = insert electron emission current, A
I_i = total ion current to cathode surfaces, A
j_i = Bohm current density, A/m^2
j_{th} = field-enhanced, thermionic emission current density, A/m^2
J = normalized emission current, see Eq. (12)
k = Boltzman's constant, 1.38×10^{-23} J/K
L_e = insert emission length, m
$\dot{m}$ = propellant mass flow rate, mA equivalent
m_i = ionic density in ion production region, kg/ion
n_e = electron density in ion production region, m^{-3}
n_i = ion density in ion production region, m^{-3}
n_0 = total neutral atom density in ion production region, m^{-3}
P = internal cathode pressure
$\dot{q}_{dx}$ = energy flux associated with de-excitation of excited states on the emission surface, W/m^2
$\dot{q}_{ph}$ = energy flux due to plasma radiation, W/m^2
Q_{th} = insert thermal power loss, W
T_e = electron temperature in ion production region, K
T_s = insert emission temperature, K
V_p = plasma potential in ion production region, V
ϵ_i = ionization potential, 10.4V for Hg
ϵ_0 = permittivity of free space, 8.85×10^{-12} F/m
ϵ_{pr} = primary electron energy, equivalent to plasma potential V_p, eV
λ_{ee} = electron-electron elastic mean free path, m
λ_{El} = effective, energy exchange, elastic mean free path for primary electrons, m
λ_{In} = effective inelastic mean free path for primary electrons, m
λ_{pr} = primary electron, energy exchange mean free path, m
ϕ_e = average effective work function, V
ϕ_s = average surface work function, V

Presented as Paper 82-1889 at the AIAA/JSASS/DGLR 11th International Electric Propulsion Conference, New Orleans, La., Nov. 17-19, 1982; revision received Dec. 14, 1983.

*Research Assistant, Department of Mechanical Engineering; presently with Ion Tech, Inc., Ft. Collins, Colo. Associate Member AIAA.

†Professor, Department of Mechanical Engineering. Member AIAA.

Introduction

THE results of previous experimental investigations of mercury orificed hollow cathodes[1,2] showed that ~70% of the total cathode current is due to surface electron emission from a narrow band (~2 mm long) on the downstream end of the low-work function insert and that the dominant surface emission process is probably that of field-enhanced thermionic emission. The results also indicated that the remaining 30% of the current is due to volume ionization that takes place in the very intense plasma discharge established adjacent to the emitting portion of the insert. A phenomenological model describing the emission and plasma production processes within the cathode was developed based on the results of those experiments.[2] The important cathode processes are shown schematically in Fig. 1. Surface electron production is from a narrow band on the downstream end of the insert, primarily from field-enhanced thermionic emission. These electrons are accelerated across the plasma sheath and thereby pick up sufficient energy to ionize mercury atoms (via multistep excitations) in the region adjacent to the insert. The total discharge current is made up of the sum of the currents due to both surface and volume electron production. The ions produced in the process leave the production volume at the Bohm velocity and are neutralized at the internal cathode potential surfaces. Ions striking the insert surface provide the energy input required to maintain the insert at the emission temperature.

By defining an idealized ion production volume as the region adjacent to the emitting portion of the insert (indicated by dashed lines in Fig. 1) and assuming that the plasma properties are uniform in that region, the physical description above can be represented analytically in a rather simple form.

The analytical model, as initially proposed, was presented in Ref. 2 and further developed in Ref. 3. The development of the model is discussed in detail in those two references, so only the important assumptions and a summary of the final results will be presented here.

Summary of Model

Table 1 gives a summary of the equations developed in the model, along with the physical basis for each equation and a brief comment indicating the important assumptions on which it is based. It should be noted that all of the equations in Table 1 are in mks units *except* the empirical expression for the pressure [Eq. (11)], where the units are as noted. Each of the equations in Table 1 will be discussed briefly below.

The total cathode discharge current I_D is the sum of the surface electron emission current I_e plus the current of volume-produced ions returning to the surface I_i. This is represented by Eq. (1) in Table 1, where j_{th} is the field-enhanced thermionic current density coming from the emitting area A_e of the insert (emission length L_e) and j_i is the Bohm current density of ions crossing the boundary of the ion production region having a surface area A_s. This equation assumes that the current due to surface emission processes such as cold-field emission, photoemission, and secondary emission due to ions and excited state atoms is negligible. These emission processes are discussed in Ref. 3, where it is shown that the electric fields at the insert surface are too low to cause appreciable field emission and that photoemission is negligible because the photons produced within the plasma by resonance de-excitations are effectively trapped due to the high neutral atom density and thus cannot reach the surface in appreciable numbers. Secondary emission currents due to ions and excited state atoms are estimated to be less than 5% of the total current, so they are also neglected. Equation (1) also neglects the electron production within the orifice region and downstream of the orifice. Experimental results indicate that

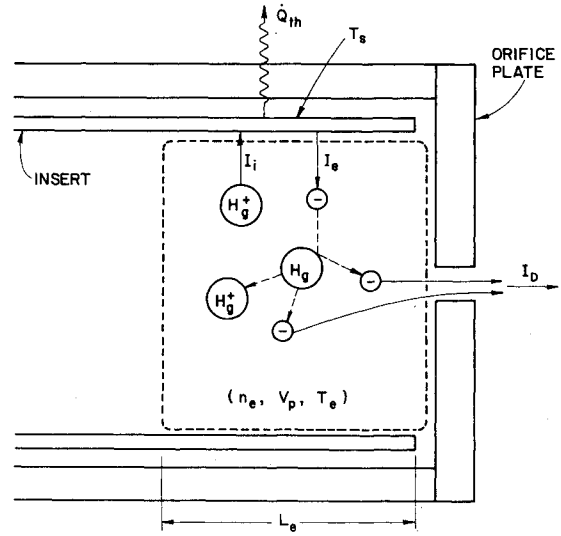

Fig. 1 Schematic of ion production engine.

Table 1 Summary of equations used in model

Physical basis	Comments	Equation	
Current balance	Thermionic electron emission from insert only; ion flux based on Bohm criterion	$I_D = I_e + I_i = j_{th}A_e + j_iA_s$	(1)
Field-enhanced thermionic emission	Model neglects all surface emission mechanisms, except this one	$j_{th} = a_0 T_s^2 \exp\left(-\frac{e\phi_e}{kT_s}\right)$	(2)
Effective work function	Based on electric field at emission surface	$\phi_e = \phi_s - \left[\frac{e\lvert E\rvert}{4\pi\epsilon_0}\right]^{1/2}$	(3)
Double-sheath analysis	Approx. based on theoretical analysis in Ref. 4. Holds for $J<10^{-3}$ [J from Eq. (1)]	$E \approx \left[\frac{n_e kT_e}{\epsilon_0}\right]^{1/2}\left[2\left(1+2\frac{eV_p}{kT_e}\right)^{1/2}-4\right]^{1/2}$	(4)
Insert energy balance	Neglects energy input due to excited states and plasma radiation	$j_i = \left[\frac{\dot{Q}_{th}}{\phi_e}+I_D\right]\cdot\left[2A_c + A_e\left(1+\frac{a}{\phi_e}\right)\right]^{-1}$ where $a=(V_p+\epsilon_i-\phi_s)$	(5)
Energy balance on ion production region	Neglects energy loss due to excited states and plasma radiation	$V_p = \frac{1}{I_D - j_iA_s}\left[\epsilon_i j_i A_s + \frac{5kT_eI_D}{2e}\right]$	(6)
Bohm criterion	Assumes uniform or average plasma properties	$n_e = j_i/e[kT_e/m_i]^{1/2}$	(7)
Existence length for primary electron	Criterion for emission/ion production region length	$L_e = 2\lambda_{pr}$	(8)
Semiempirical	Energy exchange mean free path based on results of computer model	$\lambda_{pr} = \left[\frac{6.5\times10^{-17}n_e}{V_p^2} + \frac{10^3 n_0 V_p}{2.83\times10^{23}-1.5n_0}\right]^{-1}$	(9)
Ideal gas law	Assumes heavy particle temperature equal to insert temperature	$n_0 = \frac{P - n_e k(T_e+T_s)}{kT_s}$	(10)
Empirical	Neglects orifice plate thickness effect	$P = (\dot{m}/d_0^2)(13.7+7.82I_D)\times10^{-3}$ Torr where $\dot{m}$ is in mA and d_0 in mm	(11)

this is a reasonable assumption since these sources contribute only ~7% of the total discharge current.

Equation (2) of Table 1 gives the current density j_{th} for field-enhanced thermionic emission from a surface at temperature T_s with an effective work function of ϕ_e. The effective work function ϕ_e is the surface work function ϕ_s (a material property) minus the reduction in the work function due to the electric field E at the emission surface and can be calculated using Eq. (3). The electric field in Eq. (3) is the field at the emission surface associated with the potential drop across the plasma sheath. It is estimated based on the theoretical analysis presented by Prewett and Allen[4] for the double sheath that forms at a hot cathode surface emitting electrons into a plasma. For the range of operating conditions typical of mercury hollow cathodes, Prewett and Allen's general analysis yields the approximation for the electric field given in Table 1 by Eq. (4). This approximation holds for plasmas where the ratio of plasma potential V_p to electron temperature T_e is ~10 and the normalized emission current

$$J=j_{th}\left[n_e e\left(\frac{kT_e}{m_e}\right)^{1/2}\left(2\frac{V_p}{T_e}\right)^{3/2}\right]^{-1} \tag{12}$$

is less than $\sim 10^{-3}$. These criteria are satisfied for typical cathode conditions.

The Bohm current density j_i is estimated from an energy balance on the emitting surface. In such a balance, the power due to heating from ion neutralizaton and the de-excitation of excited states is equated to the power conducted and radiated from the surface plus the power removed by emitted electrons. The equation describing this is

$$j_i A_e(V_p+\epsilon_i-\phi_s)+\dot{q}_{dx}A_e+\dot{q}_{ph}A_e=\dot{Q}_{th}+I_e\phi_e \tag{13}$$

where ϕ_e is the effective work function of the surface, ϕ_s the surface work function (a material property), $\dot{Q}_{th}$ the thermal power transferred away from the surface, V_p the potential drop across the plasma sheath, and ϵ_i the ionization potential. The terms $\dot{q}_{ph}A_e$ and $\dot{q}_{dx}A_e$ are the energy input due, respectively, to photons leaving the plasma and to surface de-excitation of the excited atomic states. The photon flux is negligible because the resonance radiation is effectively trapped within the plasma. The term $\dot{q}_{dx}A_e$ due to the excited states is believed to be relatively small, although not necessarily negligible. Calculation of this term and the various factors affecting it will be discussed in more detail in the last section of this paper. The term $\dot{Q}_{th}$ in Eq. (13) is the thermal power lost from the insert. In general, it is a function of the insert temperature T_s and must be estimated for the specific cathode thermal configuration on the basis of conduction and radiation from the insert. Neglecting the terms $\dot{q}_{dx}A_e$ and $\dot{q}_{ph}A_e$ in Eq. (13) and solving for the ion current density j_i gives Eq. (5) of Table 1. In expressing Eq. (5) in terms of the total discharge current I_D, Eq. (1) was used along with the fact that the total surface area of the ion production region is $A_s=A_e+2A_c$, where A_c is the area of the end boundary of the region.

The plasma potential is estimated by a similar energy balance on the ion production region. Energy is convected into and out of this volume by the motion of the various particle species crossing the boundaries of the ion production region. This particle motion transports not only the random and directed kinetic energy of the particles but also their excitation potential energy. Again neglecting the energy flux due to excited state atoms $\dot{q}_{dx}$ and due to radiation $\dot{q}_{ph}$ leaving the volume, the energy balance can be written simply as

$$V_p I_e=\epsilon_i I_i+\frac{5}{2}\frac{kT_e}{e}I_D \tag{14}$$

where V_pI_e is the rate at which energy is brought into the volume by the primary (surface emitted) electrons, ϵ_iI_i the rate at which energy leaves the volume in the form of ionized atoms, and $(5/2)(kT_e/e)I_D$ the rate at which energy leaves the volume due to the convection of Maxwellian electrons through the orifice [$(5/2)kT_e$ is the enthalpy of the Maxwellian electron gas]. Other energy terms such as the directed kinetic energy and enthalpy terms such as the directed kinetic energy and enthalpy of the ions and neutrals can be shown to be small[3] and are neglected. Using the current balance of Eq. (1) and solving Eq. (14) for V_p results in Eq. (6) of Table 1.

Calculation of the electric field E using Eq. (4) requires values for the plasma density n_e and the electron temperature T_e. Assuming that the plasma density ($n_e \approx n_i$) is uniform throughout the ion production region and that the ions leave the region at the Bohm velocity $(kT_e/m_i)^{1/2}$, an equation for the ion current density from the production region can be written. Rearrangement of this equation gives Eq. (7) where j_i is the ion current density from Eq. (5). The electron temperature is also needed here. However, neither Eq. (4) nor (7) is very sensitive to the electron temperature because it appears as a square root. Probe measurements in the ion production region show that, over the normal range of mercury hollow cathode operation, the electron temperature is reasonably constant at 0.71 ± 0.1 eV. Therefore, it is suggested that this measured value be used in the equations.

To complete the model, one requires a means of estimating the length of the ion production region. This length is determined by the collisional processes taking place within the ion production region. Energy input to the ion production region occurs mainly through the current of primary electrons emitted from the insert. The dominant energy exchange paths for a primary electron entering this region are inelastic collisions with a mercury atom (typically 10^9 collisions/s) and elastic collisions with Maxwellian electrons (typically 10^8 collisions/s). The elastic collision cross-section for an electron-electron collision is proportional to the inverse square of the projectile electron's energy. Therefore, once a primary electron gives up energy, by either inelastic or small-angle elastic collisions, it collision rate increases and it is rapidly thermalized; thus, the electron loses its identity as a primary The fact that primary electrons are required for the excitation reactions sustaining the plasma discharge suggests that the length of the ion production region is probably on the order of the primary electron energy exchange mean free path. Primary electrons can lose energy both by elastic collisions over a mean free path of λ_{El} and by inelastic collisions over a mean free path of λ_{In}. Therefore, the effective mean free path for the loss of a primary electron would be

$$\lambda_{pr}=(1/\lambda_{In}+1/\lambda_{El})^{-1} \tag{15}$$

From where they are created, primary electrons will to some extent be scattered upstream by elastic collisions. Therefore, a reasonable criterion for the length of the ion production region is probably one to two primary electron energy exchange mean free paths. It will be seen in the next section that a length of two mean free paths gives the best agreement with experimental results. This criterion is indicated in Table 1 by Eq.(8).

The primary electron mean free path criterion, as well as the concept of an ion production region, are clearly idealizations. In reality, the extent of the ion production region will not be sharply defined: properties will not be uniform throughout the region and ionization will occur upstream of the boundary. In addition, ions produced in the region will diffuse upstream, heating the insert in the region upstream of the boundary. So far the diffusion of ions upstream has not been discussed; although to be consistent with the model, the plasma density must fall off rapidly upstream of the boundary. If this were not the case, significant ion heating of the insert and related electron emission would be expected to occur upstream of the boundary defined by the mean free path criterion. In fact, the experimental plasma

density profiles show that the axial plasma density drops off exponentially in the upstream direction. This indicates that significant ion heating probably does not extend far upstream of the ion production region, which is consistent with the observed rapid fall off in the surface temperature upstream of the emission region. This observed behavior is also in agreement with calculations based on the ambipolar diffusion of the ions and electrons. Such calculations show that, by itself, volume recombination in the plasma can result in a density decrease upstream of the production region more rapid than that observed experimentally. In the real situation, of course, both volume ionization and wall recombination are also taking place in conjunction with volume recombination to determine the actual plasma density profile in this upstream region.

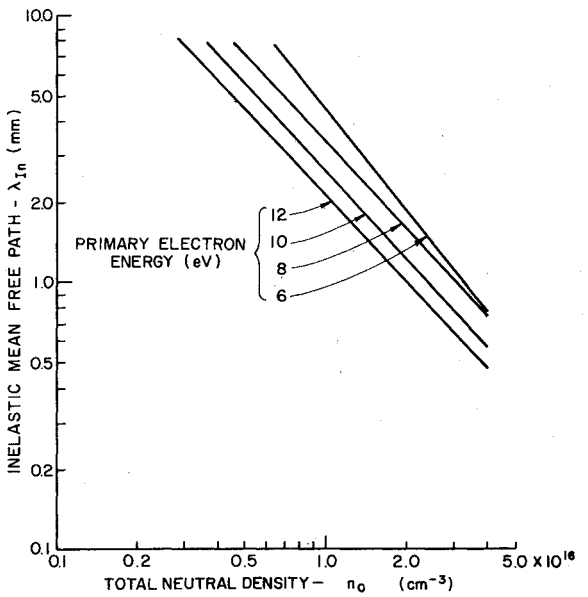

Fig.2 Effect of total neutral atom density on primary electron inelastic mean free path.

In order to use Eq. (15) to estimate the emission length it is necessary to be able to calculate the elastic (λ_{EI}) and inelastic (λ_{In}) energy exchange mean free paths. Elastic electron-ion and electron-atom collision frequencies are relatively low. Therefore, the effective elastic mean free path for energy exchange is approximately equal to the electron-electron mean free path, or

$$\lambda_{EI} \approx \lambda_{ee} = \epsilon_{pr}^2 / (6.5 \times 10^{-17} n_e) \tag{16}$$

where the expresion for λ_{ee} is based on a Coulomb collision between a primary electron with energy ϵ_{pr} and a low energy Maxwellian electron,[5] and n_e is the Maxwellian electron density. The inelastic mean free path is given by

$$\lambda_{In} = 1 \Big/ \sum_j n_\alpha \sigma_{\alpha\beta}^j \tag{17}$$

where $\sigma_{\alpha\beta}^j$ is the collision cross section for the production of excited state β from a target particle of type α having a density n_α. The summation in Eq. (17) is made over all of the important excitation reactions in the ion production region. Evaluation of γ_{In} using Eq. (17) requires the densities of the various excited states of mercury in the ion production region as well as the cross section for all of the important reactions. Peters[6] has compiled the necessary collision cross-sectional data and developed a computer model that calculates excited state densities for a mercury discharge. The application of Peters' computer model for this purpose is described in detail in Ref. 3, so only the important results will be presented here.

The computer model was used to calculate excited state densities and inelastic mean free paths λ_{In} over a wide range of input parameters typical of hollow cathode conditions. The results of the computations are shown in Fig. 2, where λ_{In} is plotted as a function of the total neutral density n_0 using primary energy as a parameter. Although all of the input parameters were varied over a considerable range, the mean free path for inelastic collisions was found to be sensitive only to total neutral density and primary electron energy. The Maxwellian electron density n_e was also found to have a slight effect on λ_{In}. However, this effect is rather small, amounting

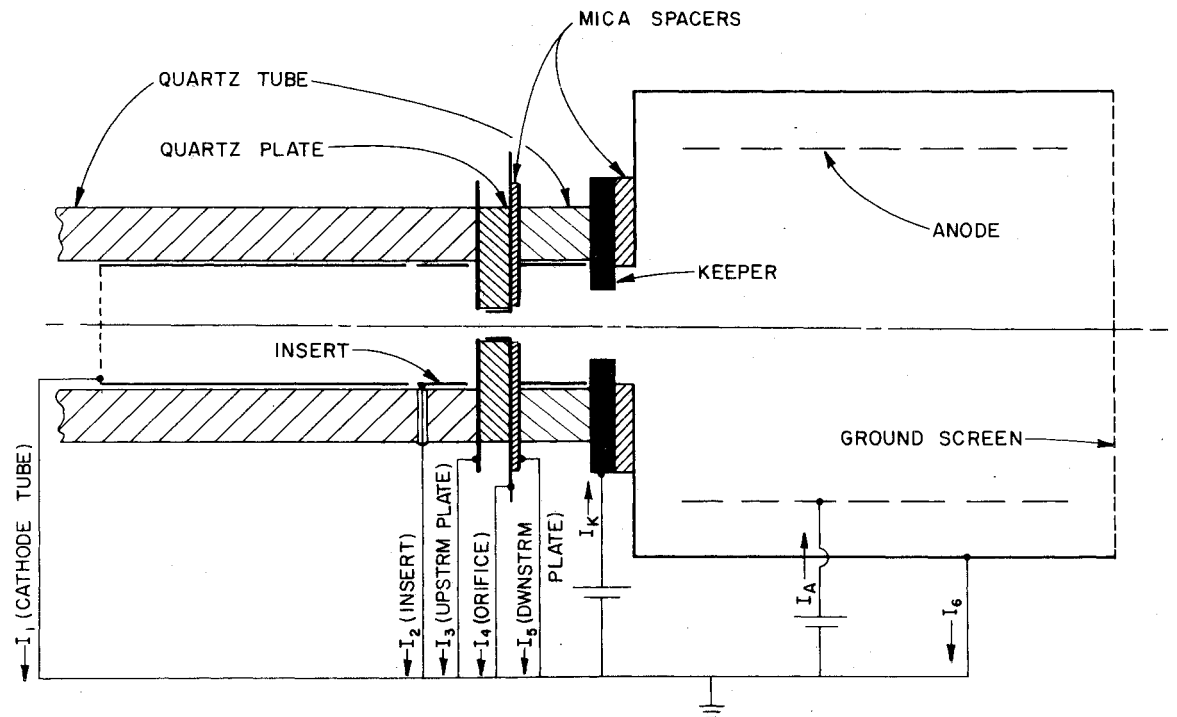

Fig. 3 Test cathode for current accounting.

to an increase in λ_{In} of less than 20% when the electron density is increased by a factor of five. For our purposes here, this effect can be neglected.

Recognizing that the mean free path varies as the inverse of the neutral density n_0, the results of Fig. 2 are fitted with the following expression

$$\lambda_{In} = \left(\frac{2.83\times 10^{23}}{n_0} - 1.5\right)\frac{1}{10^3 \epsilon_{pr}} \tag{18}$$

This expression fits the results shown in Fig. 2 within ±5% over the full range of the parameters, except for values of ϵ_{pr} equal to 6.0 V where λ_{In} is overestimated by ~20% in the intermediate density range. Using Eq. (16) for the elastic mean free path and Eq. (18) for the inelastic mean free path, the effective primary electron mean free path for energy loss due to both elastic and inelastic collisions λ_{pr} is given by Eq. (9) of Table 1. In this equation, it has also been assumed that the primary energy ϵ_{pr} is equal to the plasma potential V_p. Equation (9) provides an easy means of estimating the insert emission length. Of particular importance is the fact that over the normal range of cathode conditions, the results of Eq. (9) are dependent mainly on the neutral density and are not very sensitive to the plasma potential (V_p is normally 8-12 V) or electron density. This enables one to make a reasonable estimate of λ_{pr} based only on the typical plasma conditions and neutral density.

Finally, it is necessary to estimate the total neutral density n_0 in the region upstream of the orifice. The presence of the cathode orifice plate simplifies this problem somewhat because most of the pressure drop is across the orifice and the pressure within the cathode cavity upstream of the orifice is essentially constant. The total pressure at any point in the cathode is the sum of the partial pressures of each species. Using the ideal gas law this can be expressed as

$$P = n_e kT_e + n_i kT_i + n_0 kT_0 \tag{19}$$

where k is Boltzmann's constant, n the density, T the temperature, and the subscripts e, i, and 0 refer to electrons, ions, and neutral atoms, respectively. Given the local pressure, each of the temperatures, and the plasma density, Eq. (19) can be solved for the neutral gas density. Invoking the quasi-neutrality of the plasma (i.e., $n_e \approx n_i$) and the equilibrium of the heavy particles (ions and neutrals) with each other at the insert temperature, Eq. (19) takes the form given in Eq. (10). The local pressure P used in Eq. (10) is determined from a correlation of experimental results based on actual pressure measurements made over a wide range of mass flow rates, discharge currents, and orifice diameters.[3] This correlation is shown in Table 1 as Eq. (11), where the units are P (Torr), $\dot{m}$ (mA equivalent), d_0 (mm), and I_D(A). It is believed to be accurate to within ±30%.

Given the mass flow rate $\dot{m}$, orifice diameter d_0, insert diameter D, total discharge current I_D, surface work function ϕ_s, insert thermal power loss $\dot{Q}_{th}$, and physical constants (e, k, m_i, ϵ_0, ϵ_i, a_0), the equations in Table 1 can be solved for all of the other parameters except the electron temperature. As discussed above, a value of 0.71 eV is a reasonable assumption for the electron temperature. Because Eq. (2) cannot be solved explicitly for the surface temperature T_s, the solution of these equations is necessarily iterative. However, the equations converge to a solution very rapidly (five-place accuracy in six or seven iterations). The results of calculations based on this set of equations will be compared with experimental results in the next section.

Comparison with Experiment

An earlier paper describes an experiment in which a special quartz tube test cathode was used to determine the magnitude and origin of the various hollow cathode currents.[2] The predictions of the model will be compared here with the results of that experiment.

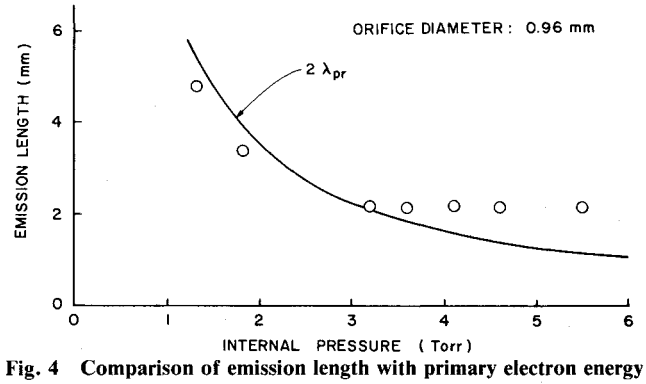

Fig. 4 Comparison of emission length with primary electron energy exchange mean free path.

A schematic of the test cathode used in the experiment is shown in Fig. 3. The cathode was fabricated from a quartz tube such that all of the internal surfaces were covered with tantalum foil and each surface of interest was isolated as a separate electrode. The insert was 2.2 mm long and had a diameter of 3.9 mm. The cathode had an orifice diameter of 0.96 mm. Both the insert and the cathode tube were coated with the low-work function chemical R-500‡. The cathode discharge was coupled to a cylindrical anode that was completely enclosed within a stainless steel ground tube covered on its downstream end by a fine mesh screen. The current from each of the surfaces shown in Fig. 3 was measured separately for total discharge currents I_D of 1.3, 2.3, 3.3, and 4.3 A at a mercury flow rate $\dot{m}$ of ~100 mA. Data were also collected for an emission current of 3.3 A at internal cathode pressures P of 1.3-5.5 Torr. The internal pressure was measured using a U-tube manometer and the insert temperature was measured using a micro-optical pyrometer.

Emission Length

A critical test of the model is its ability to predict the length of the insert emission region, since this parameter strongly affects the predicted insert surface temperature for a given discharge current and surface work function. The model assumes that the insert emission length is between one and two primary electron mean free path lengths. The primary electron mean free path λ_{pr} was calculated with Eq. (9) for the experimental conditions. In making these calculations, the neutral density was estimated from the measured cathode pressure using Eq. (10) and the primary electron energy was taken to be 8.7 eV. The primary electron energy could have been estimated using Eq. (6), but it will be seen shortly that this underestimates the plasma potential by ~2V. The value of 8.7 eV was chosen on the basis of plasma property measurements[3] showing that, over the range of normal operating conditions for this size cathode, the plasma potential in the ion production region is nearly constant at 8.7 ± 0.5 V.

The results of the mean free path calculation discussed above are plotted as the solid curve ($2\lambda_{pr}$) in Fig. 4. Insert emission lengths determined from the experimental results are indicated in the figure as circles. The agreement between the experimental data points and the calculated curve is quite good and supports the assumption of the model that $L_e/\lambda_{pr} \approx 2$. The data points above 4 Torr would have been in even closer agreement with the curve except that there was no way in this experiment to discriminate emission lengths shorter than the 2.2 mm long insert segment. Insert emission lengths, for conditions where emission was taking place not only from the insert (surface 2) but also from the cathode tube

‡A double carbonate mixture, (Ba/Sr) CO_3, manufactured by the J. R. Baker Chemical Co., Phillipsburg, N.J.

(surface 1), were estimated by assuming that the current density for emission from the tube was the same as the measured average current density of the 2.2 mm long insert at the same condition.

It is worth noting here that, for operation at a typical internal cathode pressure of ~3 Torr, the 2 mm emission length is the same as the cathode insert radius. These conditions correspond to a pressure-diameter product of ~1 Torr-cm. It is interesting to compare this with experimental results reported by Lidsky et al.[7] for an open tube cathode. Working with a number of different gases (H_2, He, A, N_2), they determined experimentally that the emission region locates itself where the local pressure-diameter product is ~1 Torr-cm. A pressure-diameter product of this magnitude corresponds to a primary electron mean free path that is on the order of the cathode radius. In the open tube cathode, the local pressure varies significantly along the tube. It is reasonable in this situation that the ion production region locates itself where conditions are such that primary electrons can reach the centerline of the cathode. In the orificed hollow cathode, on the other hand, most of the pressure drop occurs across the orifice plate, so that the pressure within the tube is rather constant along the axis of the cathode and can be adjusted independently without significantly affecting the emission location. However, a primary electron mean free path on the order of the insert radius is probably a desirable operating condition here as well. This is so even though the orificed cathode can be forced to operate under conditions with both shorter and longer primary electron mean free paths. That a primary electron mean free path on the order of an insert radius is a desirable operating condition is also suggested by experimental results[1,8] showing that a keeper/discharge voltage minimum will occur at a pressure-diameter product of a few Torr-centimeters.

The above discussion suggests that, for design purposes, the insert should be chosen to have a radius on the order of a few primary electron mean free paths. This would correspond to an insert radius about the same as the emission length and an ion production region having an aspect ratio $(D/L_e) \sim 2$. Such an aspect ratio is also convenient with regard to application of the model since it should result in an ion production region with fairly uniform plasma properties (a basic assumption of the model).

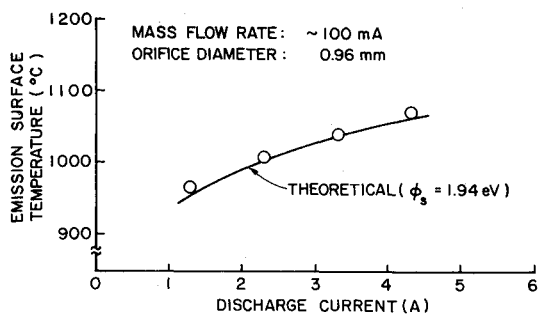

Fig. 5a Effect of discharge current on calculated and measured emission surface temperatures.

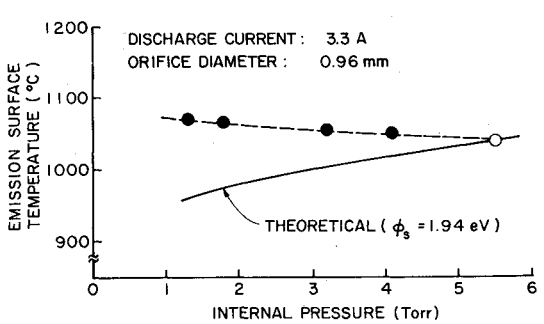

Fig. 5b Effect of internal pressure on calculated and measured emission surface temperatures.

Other Predictions

The results of the experiment can also be compared with the model's prediction of insert temperature, plasma density, and plasma potential. In order to do this, calculations using the model were performed based on the following considerations:

1) Rather than the mass flow rate, the measured pressures were used as input to the model. Equation (11) could have been used to determine the pressure from the flow rate and orifice diameter, but in this case it underestimates the pressure by about 20%. A probable explanation for this discrepancy is that the effective diameter of the tantalum, foil-lined orifice was slightly smaller during operation than its measured diameter when cold. A small error in the orifice diameter results in a large error in pressure because it appears in Eq. (11) as an inverse square.

2) The surface work function ϕ_s for the insert was not known exactly, although it was believed to be 1.8-2.0 eV. The value of 1.94 eV used in the calculation was arbitrarily chosen from this range to give agreement between the measured and calculated temperature at the operating conditions where I_D was 3.3 A and $\dot{m}$ was ~100 mA. The comparison between calculated and measured temperatures will, therefore, be a relative one valid mainly for checking the functional dependence on discharge current and pressure predicted by the model.

3) The thermal power loss used for the calculations was taken from the dashed curve of Fig. A1 in the Appendix.

4) The electron temperature was assumed to be the average measured value of 0.71 eV.

5) The ratio of emission length to mean free path L_e/λ_{pr} was assumed to be two.

The results of calculations using the model based on the assumptions discussed above are shown in Fig. 5-7. Figure 5 shows the effect of the discharge current and pressure on the emission temperatures predicted by the model for the assumed average surface work function of 1.94 eV. It should be recalled here that agreement with the experimental temperature at a current of 3.3 A was assured by selecting a value of 1.94 for ϕ_s. The significant feature of Fig. 5a, therefore, is that the model accurately predicts the effect of the discharge current on the emission temperature.

Such good agreement is not obtained for the effect of pressure on the emission temperatures. Figure 5b shows emission temperatures plotted as a function of internal pressure for a discharge current of 3.3 A. Unfortunately, at the pressure conditions indicated by the solid circles, insert temperatures were not measured in this experiment. The data indicated by the solid symbols were, therefore, estimated using the results of another experiment,[1] which showed that for a cathode of similar construction operating at a discharge current of 3.3 A the maximum insert temperature decreased by ~7°C/Torr when the internal pressure was increased. However, it is believed that this estimate is reasonably reliable, so it would not account for the differences between the two curves in Fig. 5b. The main reason for the differences between the two curves is that the temperatures indicated by the solid circles are the maximum emission temperature while the calculated temperatures (solid curves) are average values based on the assumption of uniform emission over the entire emitting length. While for short emission lengths the uniform emission assumption is probably valid, the assumption apparently breaks down as the length of the emission region increases. This suggests that, for low pressures, emission temperature gradients become important and the simple, lumped parameter model does not provide an accurate description of the emission temperature.

The ion production region plasma density predicted by the model is plotted in Fig. 6a as a function of the discharge current (solid curve). For comparison, the plasma density n_3 adjacent to the upstream side of the orifice plate is plotted as the circles. These data points (n_3) were estimated from the measured current I_3 based on the Bohm criterion [Eq. (7)] and represent the average plasma density adjacent to the downstream boundary of the ion production region. Plasma densities are shown in Fig. 6b plotted as a function of internal pressure for a discharge current of 3.3 A. In both cases (Figs. 6a and 6b), the agreement between experimental values and those predicted by the model is reasonably good, although in Fig. 6b the curve shapes for the measured and calculated values are different. This difference may be attributable, at least partially, to the assumption in the model of a uniform ion production region. This assumption is expected to hold best for operation at conditions where the primary electron mean free path is on the order of the insert radius. As the internal pressure is increased beyond this point (a few Torr), the primary elecrons have a lower probability of reaching the centerline of the cathode, so that ion production is increasingly confined to an annular region bounded by the emission surface (as opposed to the assumed cylindrical volume). Such a reduction in volume could account for the fact that the average measured values of the plasma density adjacent to the orifice plate are nearly constant for pressures above a few Torr (Fig. 6b).

The fraction of the total discharge current that is due to volume electron production processes depends mainly on the plasma density. For the plasma densities predicted by the model, this fraction was 0.30-0.34. This is in good agreement with results based on measured currents, which showed current fractions due to volume ionization of 0.27-0.31.

Finally, the plasma potential predictions of the model are shown in Figs. 7a and 7b where they are plotted, respectively, as a function of discharge current at a constant mass flow rate (~100 mA) and as a function of internal pressure at a constant discharge current (3.3A). Although the plasma potential was not measured in this experiment, results from Langmuir probe measurements made during another experiment on a similar cathode showed that the plasma potential in the ion production region was ~8.7 V.[3] The average measured value of 8.7 V from that experiment is indicated in the Fig. 7 as the dashed line. The value is shown as a constant (horizontal line) because the probe measurements indicated no clear correlation of the plasma potential in the ion production region with either current or pressure.

It should be recalled that both the plasma density and plasma potential predictions are based on energy balances for the ion production region and neglect the energy term due to the flux of excited atoms. A rough estimate of the energy flux due to the excited states was made in Ref. 3. The estimate was based on excited state densities calculated using Peters' computer model and assumed that the excited atoms leave the ion production region at their thermal velocity, carrying with them their excitation potential energy. Furthermore, it was assumed that all of the excitation energy is deposited at surfaces outside of the boundary and that the de-excited atoms return with only their random thermal energy. The excited state energy flux based on those assumptions was found to be rather large[3] and gave predictions for both plasma density and plasma potential that were not realistic. On the other hand, the results in Figs. 6 and 7 indicate that the model predicts plasma densities and plasma potentials of the right magnitude when the excited state power term is neglected. (In both cases, the model would provide better agreement if some fraction of the calculated excited state power were included, say, 0-30%.) The overestimation of the excited state energy flux may be due to a number of factors. For example, it may be that the excited state densities near the boundary and, therefore, the particle fluxes are actually overestimated. Another possibility is that the particle fluxes are estimated correctly but that there is some mechanism for returning energy to the volume, such as reflection of the

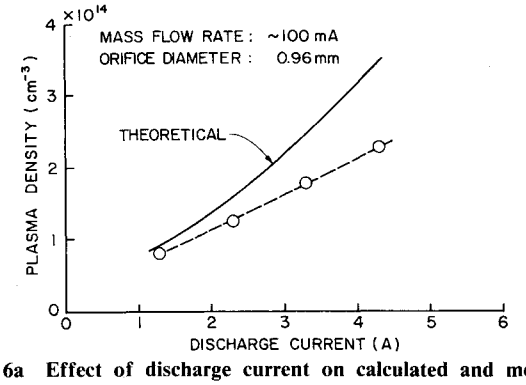

Fig. 6a Effect of discharge current on calculated and measured plasma densities.

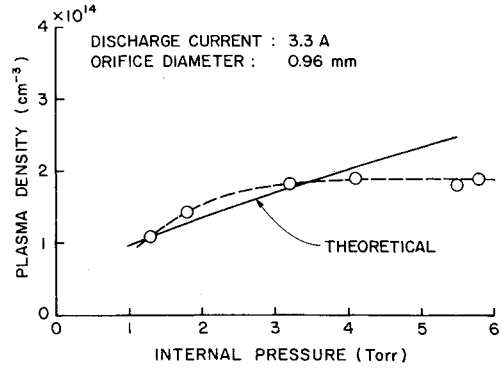

Fig. 6b Effect of internal pressure on calculated and measured plasma densities.

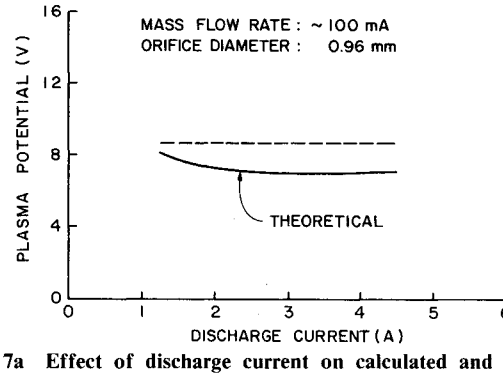

Fig. 7a Effect of discharge current on calculated and measured plasma potentials.

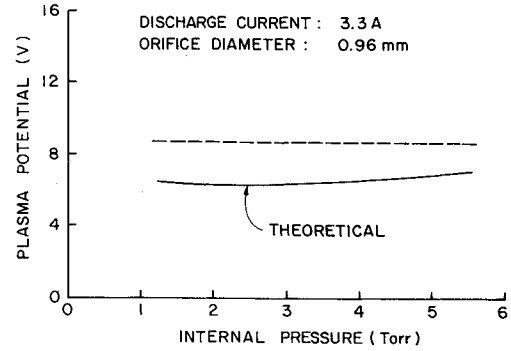

Fig. 7b Effect of internal pressure on calculated and measured plasma potentials.

excited particles or of resonance radiation from the cathode surfaces. However, even in light of these uncertainties associated with calculation of the excited state energy flux, the model provides a useful and reasonable qualitative description of the basic physical processes taking place within the cathode.

Based on the above experimental results, it is suggested that for design purposes the average measured values of the electron temperature (0.71 eV) and plasma potential (8.7 V) should be used when making calculations with the model. The results also indicate that the best agreement between model and experiment is obtained when the ion production region aspect ratio (D/L_e) is on the order of 2. This is also a condition that is expected to provide good cathode performance.

Conclusions

A phenomenological model has been presented that describes the physical processes underlying the operation of mercury orificed hollow cathodes of the type used in ion thrusters. This descriptive model is in good qualitative agreement with the experimental results, indicating that our basic understanding of the important physical processes for these devices is essentially correct. By assuming an idealized ion production region within which most of the plasma processes are concentrated, this phenomenological model has been expressed analytically as a simple set of equations relating the cathode dimensions and specifiable operating conditions, such as mass flow rate and discharge current, to such important parameters as the insert temperture and plasma properties. Comparison with experimental results shows that, if the excited state energy flux is neglected, the model provides reasonably accurate predictions of emission length, emission surface temperature, plasma density, and fraction of discharge current due to volume ionization. The plasma potential prediction of the model is rather low; and it is suggested that the average measured value of 8.7 V be used in place of Eq. (6) when making calculations using the model. An ion production region aspect ratio (D/L_e) of 2 is suggested as a design criterion for minimizing keeper voltage.

Appendix: Thermal Power Loss from Emission Surface

The rate of heat transfer $\dot{Q}_{th}$ away from the emitting portion of the insert due to conduction, convection, and radiation is required for the energy balance calculations discussed above. An accurate value for the power loss $\dot{Q}_{th}$ for the experimental cathode is not easily determined, although bounds can be placed on its value and a reasonable estimate can be made. A maximum value can be determined by assuming that the end of the quartz tube holding the insert segment is at the same temperature as the segment (perfect thermal contact). The power loss is then calculated based on conduction down the quartz tube and radiation from its outer surface to ambient ($T_a \approx 300$ K). The quartz tube would then be analogous to a cylindrical fin, one end of which is at the insert temperature. The results of this analysis are plotted in Fig. A1 as a function of insert temperature and are indicated by the upper (maximum) curve. The minimum value of $\dot{Q}_{th}$ is calculated by assuming radiation from both outer and inner surfaces of the insert to the surfaces at 700°C and by neglecting all losses due to conduction and convection from the insert. A temperature of 700°C was selected because the adjacent surfaces (nonemitting portion of insert, startup heater, etc.) were at a temperature less than the minimum

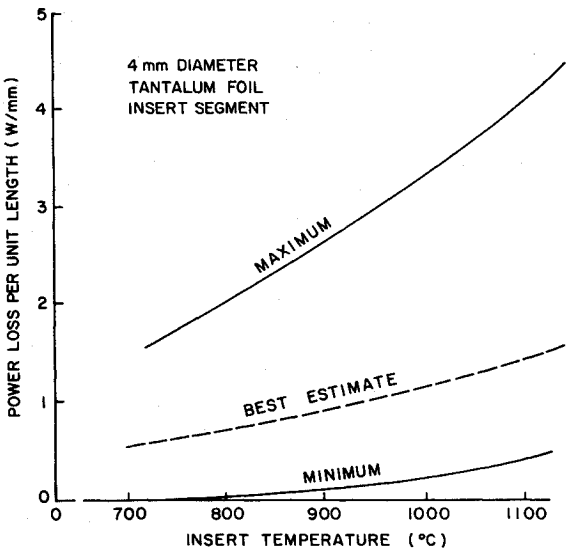

Fig. A1 Thermal power loss for 2 mm long tantalum foil insert segment.

temperature detectable with the optical pyrometer (~700°C) used in making the temperature measurements. The minimum value for $\dot{Q}_{th}$ calculated in this way is plotted as the lower curve in Fig. A1. Finally, a more probable value for $\dot{Q}_{th}$ is calculated by assuming direct radiation from the insert in addition to some contact betweeen the insert and the quartz tube. The heat transfer between the insert and tube is estimated to be due to a combination of direct contact and transfer via the intervening mercury vapor. The heat transferred to the tube is then assumed to be conducted down its length and radiated from its median diameter to surfaces at $T_a \approx 300$ K. The results of this analysis are plotted in Fig. A1 as the dashed (best estimate) curve.

Acknowledgment

This work was performed under NASA Grant NGR-06-002-112.

References

[1] Siegfried, D.E. and Wilbur, P.J., "Studies on an Experimental Quartz Tube Hollow Cathode," AIAA Paper No. 79-2956, Oct. 1979.

[2] Siegfried, D.E. and Wilbur, P.J., "A Phenomenological Model Describing Orificed Hollow Cathode Operation," AIAA Paper 81-0746, April 1981.

[3] Siegfried, D.E., "A Phenomenological Model for Orificed Hollow Cathodes," Doctoral Dissertation, Colorado State University, Fort Collins, Dec. 1982.

[4] Prewett, P.D. and Allen, J.E., "The Double Sheath Associated with a Hot Cathode," *Proceedings of the Royal Society of London,* Ser. A, Vol. 348, No. 1655, April 1976, pp. 435-446.

[5] Jahn, R.G., *Physics of Electric Propulsion,* McGraw Hill Book Co., New York, 1968, Chap. 4.

[6] Peters, R.R., "Double Ion Production in Mercury Thrusters," NASA CR-135019, April 1976.

[7] Lidsky, L.M., Rothleder, S.D., Rose, D.J., Yoshikawa, S., Michelson, C. and R.J. Macken, Jr., "Highly Ionized Hollow Cathode Discharge," *Journal of Applied Physics,* Vol. 33, Aug. 1962.

[8] Martin, R.J. and Rowe, J.E., "Experimental Investigation of the Low-Voltage Arc in Noble Gases," *Journal of Applied Physics,* Vol. 39, Aug. 1968, pp. 4289-4298.